Fragile spin liquid in three dimensions

Anna Fancelli,[1,2,*] R. Flores-Calderón,[3,4,*] Owen Benton,[5] Bella Lake,[2,6] Roderich Moessner,[3] and Johannes Reuther[1,2]

[1]*Dahlem Center for Complex Quantum Systems and Fachbereich Physik, Freie Universität Berlin, Arnimallee 14, 14195 Berlin, Germany*

[2]*Helmholtz-Zentrum Berlin für Materialien und Energie GmbH, Hahn-Meitner-Platz 1, 14109 Berlin, Germany*

[3]*Max Planck Institute for the Physics of Complex Systems, Nöthnitzer Strasse 38, 01187 Dresden, Germany*

[4]*Max Planck Institute for Chemical Physics of Solids, Nöthnitzer Strasse 40, 01187 Dresden, Germany*

[5]*School of Physical and Chemical Sciences, Queen Mary University of London, London E1 4NS, United Kingdom*

[6]*Institut für Festkörperforschung, Technische Universität Berlin, 10623 Berlin, Germany*

(Received 7 November 2024; revised 24 March 2025; accepted 28 March 2025; published 9 April 2025)

Motivated by the recent appearance of the trillium lattice in the search for materials hosting spin liquids, we study the ground state of the classical Heisenberg model on its line graph, the trilline lattice. We find that this network realizes the recently proposed notion of a fragile spin liquid in three dimensions. Additionally, we analyze the Ising case and argue for a possible $\mathbb{Z}_2$ quantum spin liquid phase in the corresponding quantum dimer model. Like the well-known $U(1)$ spin liquids, the classical phase hosts moment fractionalization evidenced by the diluted lattice, but unlike those, it exhibits exponential decay in both spin correlations and interactions between fractionalized moments. This provides an instance of a purely short-range correlated classical Heisenberg spin liquid in three dimensions.

DOI: 10.1103/PhysRevB.111.134413

I. INTRODUCTION

The interplay between frustration, topology, and strong interactions has opened a window into the limits of what matter can be and do. Because of their exotic properties, spin liquids represent natural settings for such explorations [1–6]. Recently, much work has been done on the forefront of generalizing the low-energy theory from conventional gauge theories to higher-rank gauge theories [7–20]. An example is the recently theorized rank-2 $U(1)$ spin liquid, which is described by a traceless symmetric tensor instead of the usual vector potential of electromagnetism. These exotic extensions to our fundamental theories are not realized in our universe, so their study and realization may unravel physical effects that cannot otherwise be studied.

On another front, a recent classification scheme for classical spin liquids (CSLs) was put forward, and the notion of a fragile spin liquid (FSL) was introduced in [21,22]. This type of spin liquid is a phase of matter defined by the presence of fractionalization and the absence of algebraic correlations. Its description encompasses a disordered phase with no magnetic ordering and extensive ground-state entropy. Within the approach used in [21,22] the topological invariants associated with the flat bands of the interaction matrix that classify such FSLs can change if additional degrees of freedom are introduced in the unit cell. The idea of such a short-range correlated state is not new. We may recall the quintessential example for a strongly correlated topological phase of matter, the toric code. Originally defined in the square lattice, this model presents fractionalized excitations in the form of emergent electric and magnetic particles with semionic statistics [23–26]. The exactly known ground state has a gap to excited states realizing the celebrated $\mathbb{Z}_2$ topological order. In a similar spirit we present here an instance of a three-dimensional (3D) fragile spin liquid which acts as a classical analog to the $\mathbb{Z}_2$ quantum spin liquids.

The theoretical identification of novel spin liquids is also of high experimental relevance, given the lack of conclusive physical spin liquid realizations and the quest to identify experimentally relevant signatures. Recently, it was proposed that a classical Heisenberg model on the distorted windmill lattice, inspired by the spin-1/2 spin liquid candidate $PbCuTe_2O_6$ [27], exhibits an extensive ground-state degeneracy characteristic of classical spin liquid behavior [28]. For a particular arrangement of spin couplings this CSL can be understood as a spin model on the line graph of the trillium lattice, which we name the *trilline lattice*. While the trillium lattice consists of a noncentrosymmetric network of corner-sharing equilateral triangles, the trilline lattice consists of distorted corner-sharing octahedra. Of particular relevance is its characteristic nonbipartite structure, which is known in two dimensions to change the nature of the frustrated magnetic phase. We may compare this situation to the well-known case

*These authors contributed equally to this work.

Published by the American Physical Society under the terms of the Creative Commons Attribution 4.0 International license. Further distribution of this work must maintain attribution to the author(s) and the published article's title, journal citation, and DOI. Open access publication funded by Max Planck Society.

of spin ice, described by the pyrochlore lattice, a network of corner-sharing tetrahedra, which permits a bipartite lattice description. This property together with the spin ice constraint of vanishing net spin on each tetrahedron ultimately leads to its remarkable $U(1)$ gauge structure.

In contrast, previous works noted that for Ising spins in a nonbipartite lattice, sectors of the configuration space are labeled by $\mathbb{Z}_2$ winding parities rather than the $\mathbb{Z}$-valued winding numbers of $U(1)$ gauge theories realized on bipartite lattices [29]. When translated to the disordered dimer coverings on nonbipartite lattices, it was found that the entropic interaction potential between a pair of monomers approaches a finite limiting value exponentially fast with increasing separation [30–32]. The deconfinement of monomers is a telltale sign of fractionalization; however, dimer-based descriptions are natural for discrete Ising spins, while the dilution signatures studied in this paper can be more generally applied to other spin models, particularly continuous ones [33–35], and even to the quantum versions of these models [36].

The rest of this paper is structured as follows. In Sec. II we describe our spin model on the trilline lattice and its relation to previously studied frustrated models. Next, in Sec. III, we characterize the spin correlations via the structure factor in momentum space and analyze how our model fits in the recently introduced classification of CSLs [21,22]. In Sec. IV we probe the fractionalization properties of the system via the introduction of nonmagnetic vacancies, and we find that the most relevant dilution clusters behave as free spins with a fractional magnetic moment of $S/2$. Together with exponentially decaying correlations between the dilution clusters, the analog of gauge charges, this distinguishes gapped 3D $\mathbb{Z}_2$ spin liquids from algebraic ones and positions them as an instance of fractionalization with purely short-range correlations. Finally, in Sec. V we discuss the Ising version of our spin model on the trilline lattice, which we rewrite as a dimer model, and elaborate on the effects of dimer resonances. We argue that such resonances can be tuned to a point of genuine *quantum* spin liquid behavior, known as the Rokhsar-Kivelson (RK) point. We end with a conclusion in Sec. VI.

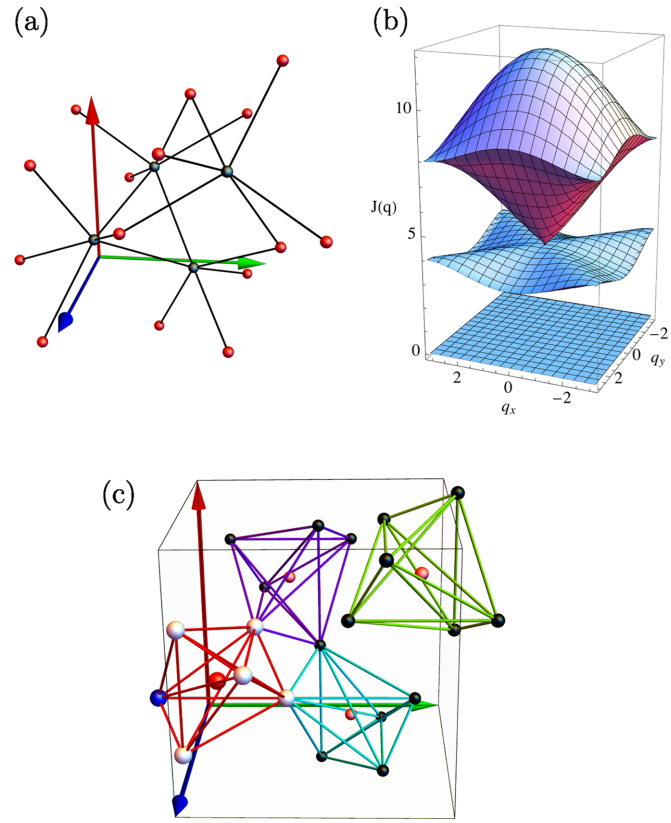

FIG. 1. (a) Trillium lattice, with the four unit cell sites shown in gray and the corresponding nearest-neighbor sites shown in red. We note that the site positions of the trillium lattice depend on one real parameter. The details of the specific realization used in this work are given in Appendix B. (b) Dispersion of the interaction matrix eigenvalues in SCGA in the $q_z = 0$ plane. (c) Unit cell with the four inequivalent octahedra of the trilline lattice shown in distinct colors. A collection of vacancy spins (white) yields an orphan spin (blue). The centers of the octahedra (red spheres) correspond to the trillium lattice.

II. MODEL

We consider classical $O(3)$ Heisenberg spins in the line graph of the trillium lattice with the Hamiltonian

$$\mathcal{H} = \frac{J}{2} \sum_{\text{oct}} \left(\sum_{i \in \text{oct}} \vec{S}_i \right)^2, \tag{1}$$

where oct refers to the distorted octahedral cages of the line graph of the trillium lattice [Fig. 1(a)], which we call the trilline lattice. The trillium lattice [37] from which the trilline lattice is constructed is a lattice with a four-atom cubic unit cell consisting of corner-sharing equilateral triangles, where each lattice site is part of three triangles.

A line graph is constructed by considering the midpoints of all the nearest-neighbor bonds for each distinct point in the original graph, here forming the distorted octahedral cages [see Fig. 1(c)]. As also illustrated in Fig. 1(c), the centers of the distorted octahedra are the sites of the trillium lattice, and thus, the trillium lattice is the dual to the nonbipartite trilline lattice when we consider the dual graph to be built from the centers of the elementary two-chains. The practical construction of the trilline lattice, along with the Heisenberg couplings required for the Hamiltonian in Eq. (1), is explained in Appendix B.

Below we investigate the properties of the model (and a diluted version thereof) in a large-$\mathcal{N}$ approximation, also known as the self-consistent Gaussian approximation (SCGA) [34,35,38–40], where the number of spin components is generalized from three to $\mathcal{N}$; see Appendix C for the details of the method. Within this formalism we consider the interaction matrix $J(\mathbf{q})$ in momentum space, which allows us to rewrite the Hamiltonian in Eq. (1) as

$$\mathcal{H} = \frac{1}{2} \sum_{\mathbf{q}} \sum_{a,b=1}^{n} \tilde{S}_a(-\mathbf{q}) J_{ab}(\mathbf{q}) \tilde{S}_b(\mathbf{q}), \tag{2}$$

where we have defined the Fourier transformed spin field $\tilde{S}_b(\mathbf{q})$ and $n = 12$ is the number of sublattices in the trilline lattice.

Diagonalizing the matrix $J_{ab}(\mathbf{q})$ results in a spectrum which contains eight degenerate bottom flat bands and four dispersing ones with a linearly dispersing cone at finite energy and zero momentum separated by a gap, as shown in Fig. 1(b). This band-touching point is a Weyl point which has a corresponding partner at the Brillouin zone corner (π, π, π), consistent with the fact that only an even number of Weyl points is allowed in lattice models. This feature is interesting in itself, as it suggests a nontrivial source of Berry curvature from each Weyl point, which may be an analog to the topological Weyl magnons and would be of much interest to the magnetism and transport community [41].

It is worth noting that the ground-state flat bands are of crucial importance for the existence of a spin liquid phase. Physically, such zero modes represent the allowed transformations which keep the ground-state constraint, $\sum_{i\in\text{oct}} \vec{S}_i = 0$, implied by Eq. (1) intact. This ground-state constraint results in an extensively large number of ground states. This extensive degeneracy reflects the presence of flat bands, as is the case for a classical spin liquid. In contrast, the upper dispersive bands represent the configurations which violate the ground-state constraint. These excited states are usually not in a simple relationship to the flat band states. However, in algebraic spin liquids like the $U(1)$ spin ice, the excited states of the dispersive bands can be understood as the charges of the emergent gauge theory added to the ground states.

III. CHARACTERIZATION OF THE SPIN LIQUID PHASE

To analyze the ground-state phase of our model we consider the static structure factor, defined as

$$\mathcal{S}(\mathbf{q}) = \langle \vec{S}(\mathbf{q}) \cdot \vec{S}(-\mathbf{q}) \rangle. \tag{3}$$

If the system were magnetically ordered, we would see the presence of sharp Bragg peaks at specific momentum points. Instead, we see only smooth, broad features as exemplified in Fig. 2, which displays cuts of the 3D Brillouin zone along two planes. Within the SCGA [see Fig. 2(a)] we may compute the spin structure factor for low enough temperatures simply as the projector to the flat bands $\mathcal{S}(\mathbf{q}) = \mathcal{P}_{\text{flat}}(\mathbf{q})$, which in our case are eightfold degenerate. The absence of Bragg peaks indicates no ordering to the lowest temperatures, while the absence of pinch-point singularities, which are quintessential of spin ice [39,42–46], further confirms the short-range exponentially decaying correlations of the spins. We simulate the three-component ($\mathcal{N} = 3$) Heisenberg system using classical Monte Carlo (MC) methods (see Appendix A for details). Throughout, energy and temperature are expressed in units of J, with $J = 1$. The spin structure factor obtained from MC simulations, shown in Fig. 2(b), exhibits a signal distribution qualitatively similar to the one obtained from SCGA in Fig. 2(a), with no peaks or other singularities.

Further characterization of the spin liquid phase can be obtained by studying the constraint of the Hamiltonian using the methods and classification described in detail in Refs. [21,22], which we follow next. Our goal will be to identify to which class of momentum-space mappings our model belongs within this classification scheme. We conjecture and later show by means of dilution that our model belongs to a fractionalized phase. Let us start by defining the constrainer,

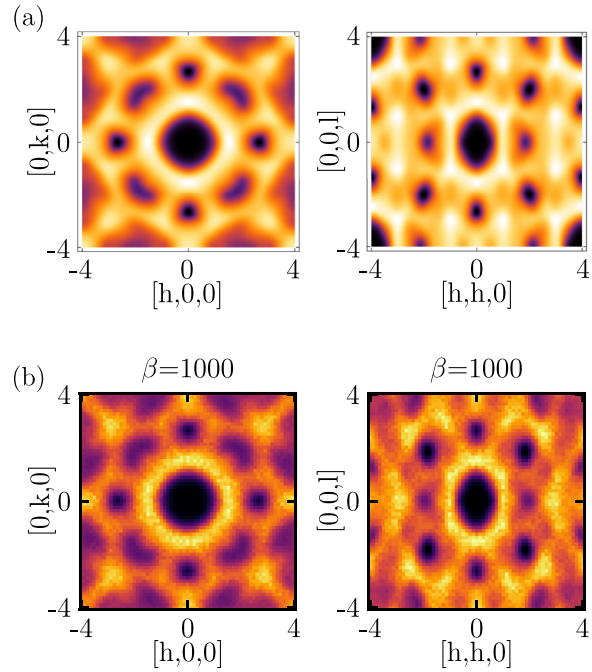

FIG. 2. Static spin structure factor $\mathcal{S}(\mathbf{q})$ calculated within (a) the SCGA scheme for the $(h00)$ plane vs the $(0k0)$ plane and for the $(hh0)$ plane vs the $(00l)$ plane. (b) Analogous plots for the Heisenberg case obtained from MC simulations at the lowest simulated temperature, corresponding to $\beta = 1000$.

which is a sum of spins that is zero in the ground state, thus constraining the possible ground-state spin configurations. We note first that the unit cell has four octahedra, as shown in Fig. 1(a), which means that we have $m = 4$ constrainers and $n = 12$ sublattices, implying $n - m = 8$ flat bands, as mentioned previously. We write the Hamiltonian in the constrainer form:

$$\begin{aligned}\mathcal{H} &= \frac{J}{2} \sum_{\mathbf{R}\in \text{u.c.}} \sum_{I=1}^{m} [\mathcal{C}_I(\mathbf{R})]^2 \\ &= \frac{J}{2} \sum_{\mathbf{R}\in \text{u.c.}} \sum_{I=1}^{m} \left[\sum_{\mathbf{r}} \mathbf{S}(\mathbf{r}) \cdot \mathbf{C}_I(\mathbf{R}, \mathbf{r}) \right]^2 .\end{aligned} \tag{4}$$

In the first line, $\mathcal{C}_I(\mathbf{R})$ denotes the constrainers of our model. For a unit cell (u.c.) at position $\mathbf{R}$ and for an octahedron I within that unit cell the constrainer $\mathcal{C}_I(\mathbf{R}) = \sum_{i\in\text{oct}(\mathbf{R},I)} S_i$ [47] is the sum of spins in this octahedron, indicated by the notation $i \in \text{oct}(\mathbf{R}, I)$. In the second line of Eq. (4) this sum is rewritten using a vector notation over sublattices with $\alpha = 1, \ldots, 12$, where $\mathbf{S}(\mathbf{r}) = (S_1(\mathbf{r}), \ldots, S_{12}(\mathbf{r}))$ and $\mathbf{r}$ denotes the positions of the spins. The entries of $\mathbf{C}_I(\mathbf{R}, \mathbf{r})$ are $C_I^\alpha(\mathbf{R}, \mathbf{r}) = 1$ if the octahedron I in the unit cell $\mathbf{R}$ has a site on sublattice α and if $\mathbf{r}$ matches the position of that site. In all other cases $C_I^\alpha(\mathbf{R}, \mathbf{r}) = 0$. By Fourier transforming we obtain the so-called Fourier-transformed (FT) constrainers denoted by $\mathbf{T}_I(\mathbf{q}) = \sum_{\mathbf{r}} \mathbf{C}_I(\mathbf{R}, \mathbf{r}) e^{i\mathbf{q}\cdot\mathbf{r}}$. The FT constrainers span the eigenspace of all nonflat bands; in our case we have $m = 4$ of these bands. We further identify vectors $\mathbf{T}_I(\mathbf{q})$ which differ by a complex number, $\mathbf{T}_I(\mathbf{q}) \sim c\,\mathbf{T}_I(\mathbf{q})$, with $c \in \mathbb{C}$ since they correspond to the same spin configurations. This

reduces the $n = 12$ dimensional complex vector space of the FT constrainers to the complex projective space $\mathbb{C}P^{n-1}$.

Using the fact that the topology of the Brillouin zone is that of a three-torus, we focus on mappings from T^3 to a subset of $\mathbb{C}P^{11}$ generated by $\mathbf{T}_1(\mathbf{q})$, $\mathbf{T}_2(\mathbf{q})$, $\mathbf{T}_3(\mathbf{q})$, and $\mathbf{T}_4(\mathbf{q})$. The space of all m-dimensional subspaces in $\mathbb{C}P^{n-1}$ is known as the complex Grassmanian, denoted by $\mathrm{Gr}(m, n)$. For a single dispersive band $\mathrm{Gr}(1, n) = \mathbb{C}P^{n-1}$, as expected [21]. In our case $m = 4$, and $n = 12$, so the appropriate space to consider is $\mathrm{Gr}(4, 12)$. Since calculating the homotopy group $[T^3, \mathrm{Gr}(4, 12)]$ and determining whether our model falls into a topologically nontrivial class is an arduous task, we choose instead to focus on the physically relevant signatures that we would expect in such a case. If we find an observable that takes a distinctly different value than that for a trivial paramagnet, we can conjecture that our system lies in a topologically nontrivial sector. In the following, we identify such an observable as the emergent magnetic moment of certain dilution clusters.

IV. DILUTION AND FRACTIONALIZATION

To further probe the emergent cooperative behavior of our system, we study the response to nonmagnetic vacancies in the form of dilution. The simplest case is that of a single spin being removed from a given octahedron. Starting from the ground state of the Hamiltonian in Eq. (1), we observe that the total magnetization in each distorted octahedron must be zero. The effect of removing a single spin can then be compensated by rearranging the remaining spins such that the local ground-state constraints are still fulfilled. Such a smooth deformation is allowed by the continuous $O(3)$ nature of the spins. Hence, we do not expect a single missing spin to significantly change the bulk response.

This argument can be extended to multiple spins being removed from a single cluster until all but one of its spins have been removed. Such a configuration implies $\vec{S}_{\mathrm{oct}} = \sum_{i\in\mathrm{oct}} \vec{S}_i \equiv \vec{S}_{\mathrm{O}} \neq 0$, where $\vec{S}_{\mathrm{O}}$ is the last remaining *orphan spin* in this octahedron. An example of such a dilution configuration is shown in Fig. 1(c), where we illustrate the missing sites using white spheres, show the centers of the distorted octahedra as red spheres, and draw the bonds in the different octahedra in different colors. Furthermore, the orphan spin is shown in blue. Because of the hard spin length constraint, there is no possibility of smoothly compensating this dilution. An orphan spin cluster will thus dominate the magnetic response at low temperatures. This can be seen from its free-spin behavior, but it has a fractional spin magnitude, which implies a diverging susceptibility contribution at zero temperature, as noted in Ref. [33].

Moreover, we can understand these dilution clusters from the perspective of low-energy theory. In the usual case of $U(1)$ spin liquids such configurations violate the local gauge constraint, and we can think of them as chemically placed gauge charges. In fact, it is known that such configurations probe the emergent fractionalization properties of other spin liquids as well [20,29,33,48]. This property of fractionalization in a fragile spin liquid differs from conventional Coulomb spin liquids, quantum or classical. In our case, the low-energy theory does not satisfy an emergent Gauss law. Previous studies found that in the Ising case [29] one can reformulate the dimer covering problem and find that the low-energy theory is that of a gauge theory with charge 2 matter. Nevertheless, this does not apply generally; in particular, there is no such known reformulation for the Heisenberg models.

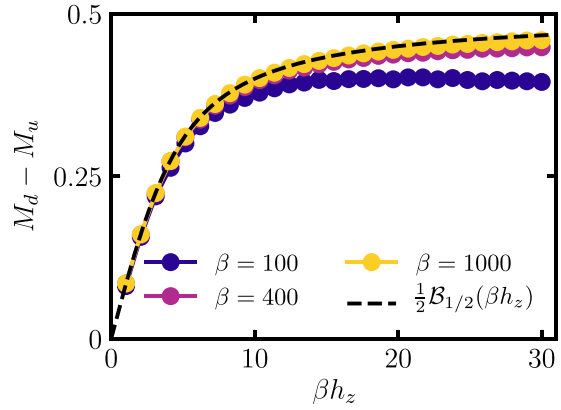

FIG. 3. Magnetization of the diluted system M_d (one orphan spin) minus that of the undiluted case M_u as a function of inverse temperature and magnetic field from classical MC. We fix the temperature and scan the magnetic field. The black dashed line shows the theoretical value for a fractionalized moment of 1/2, given by the Brillouin function $\mathcal{B}_s(h_z\beta)$ times S for $S = 1/2$. This function describes the magnetization of a paramagnet with magnetic moment S in response to an external magnetic field.

A. Fractional magnetic moment

The trilline lattice is composed of corner-sharing distorted octahedra. Crucially, this implies that we can write the Hamiltonian in a magnetic field $\vec{h}$ as

$$\mathcal{H} = \frac{J}{2}\sum_{\mathrm{oct}}\left(\sum_{i\in\mathrm{oct}}\vec{S}_i\right)^2 - \sum_i \vec{h}\cdot\vec{S}_i \tag{5}$$

$$= \frac{J}{2}\sum_{\mathrm{oct}}\left(\sum_{i\in\mathrm{oct}}\vec{S}_i\right)^2 - \frac{1}{2}\sum_{\mathrm{oct}}\sum_{i\in\mathrm{oct}}\vec{h}\cdot\vec{S}_i \tag{6}$$

$$= \frac{J}{2}\sum_{\mathrm{oct}}\left(\sum_{i\in\mathrm{oct}}\vec{S}_i - \frac{\vec{h}}{2J}\right)^2 + \mathrm{const.} \tag{7}$$

Since an orphan spin in a specific octahedron oct implies $\sum_{i\in\mathrm{oct}}\vec{S}_i \equiv \vec{S}_{\mathrm{O}}$, expanding the first term in Eq. (7) yields a contribution from this octahedron $\mathcal{H}_{\mathrm{O}} = -\frac{1}{2}\vec{h}\cdot\vec{S}_{\mathrm{O}}$. This can be read as a reduced magnetic moment of a free spin of magnitude $\alpha S = S/2$. This argument assumes a certain independence between the spin clusters and could still be interpreted as a reduction of the magnetic field instead of a change in magnetic moment. Nevertheless, from our MC simulations and the more involved vacancy field theory (FT), we find that the behavior for small fields and low temperatures is, indeed, quantitatively described by a free $S/2$ magnetic moment, as shown in Fig. 3. There, we plot the diluted minus the undiluted magnetization from MC as a function of βh_z for fixed temperatures.

As a final note, the magnetic moment found here fractionalizes with the specific value $S/2$. It has been shown that

the magnetic moment of such an orphan spin can be tuned continuously and can even assume irrational values while staying in the spin liquid phase [20]. However, such a tunable moment was found in *gapless* rank-1 and rank-2 $U(1)$ spin liquids. We expect that for a gapped fragile phase such as the one studied here the value of the fractional magnetic moment may change but cannot be deformed to a trivial value without closing the gap. As shown above, the exact value for the magnetic moment in our model is determined from the fact that we have corner-sharing octahedra giving a magnetic moment of $S/2$. Furthermore, the quantum Heisenberg model can retain the magnetic moment fractionalization even if it has an ordered ground state, as long as we focus on a thermal window between the ordering temperature and the interaction spectrum gap, as shown previously in the kagome case [36].

B. Orphan spin correlations

Next, we consider the case of two vacancy clusters, with each one containing an orphan spin, $\vec{S}_{O_1}(\mathbf{r}_1)$ and $\vec{S}_{O_2}(\mathbf{r}_2)$ at positions $\mathbf{r}_1$ and $\mathbf{r}_2$. We calculate the spin-spin correlations between the orphan spins as a function of their distance. As shown in Fig. 4, we find from both FT and MC an exponential decay in the correlations,

$$\langle \vec{S}_{O_1}(\mathbf{r}_1) \cdot \vec{S}_{O_2}(\mathbf{r}_2) \rangle \propto e^{-|\mathbf{r}_1-\mathbf{r}_2|/\xi}, \tag{8}$$

where the distance $|\mathbf{r}_1 - \mathbf{r}_2|$ is defined as the number of bonds between the two orphans. This is highly unusual since for typical Coulomb spin liquids we would obtain in three dimensions a $1/|\mathbf{r}_1 - \mathbf{r}_2|$ decay characteristic of the charges being interpreted as charges of the emergent gauge field [33–35,39,42,44,49]. Intuitively, we can understand the exponential decay from the fact that the FT constrainers, $\mathbf{T}_I(\mathbf{q}) = \sum_{\mathbf{r}} \mathbf{C}_I(\mathbf{R}, \mathbf{r}) e^{i\mathbf{q}\cdot\mathbf{r}}$, are nonzero across the Brillouin zone since the system is gapped. An expansion around the high-symmetry point Γ leads to a mass term at zeroth order, $T_I^{\alpha}(\mathbf{q} = 0) = \sum_{i\in\alpha, i\in I}$, of order 1. This means that the correlation length ξ is also of order 1 in units of the lattice spacing, and indeed, in our MC simulations we find that correlations in most directions are almost zero for distances beyond one unit cell.

V. ISING AND QUANTUM DIMER MODEL

Let us briefly discuss the fate of our model for discrete Ising (rather than continuous Heisenberg) spins. We are interested in this case since it is the simplest limit where perturbations can be understood within a fully quantum mechanical description. The Ising Hamiltonian with discrete Ising spins S_i^z for each point of the trilline lattice can be written in the same way as in Eq. (1). The ground states of this Hamiltonian are configurations where the total spin in each distorted octahedron is zero, which means that three spins point up and three spins point down. There are 20 possible configurations per octahedron satisfying this ice rule, which suggests an extensively degenerate ground state. Let us show this more explicitly within the independent octahedra (Pauling) approximation. A system with N Ising spins can be in 2^N different configurations. In each octahedron there are $\binom{6}{3} = 20$ ground states out of the 2^6 possible spin configurations. Each octahedron has six spins which are all shared between two octahedra such that the total number of octahedra is $N/3$, leading to $2^N \times (\frac{20}{2^6})^{N/3} = (\frac{5}{2})^{N/3}$ ground-state configurations. The expected entropy at zero temperature is then $S = \frac{N}{3}\ln(\frac{5}{2}) \approx 0.3\ N$, about 50% more than the residual entropy of spin ice on the pyrochlore lattice of corner-sharing tetrahedra.

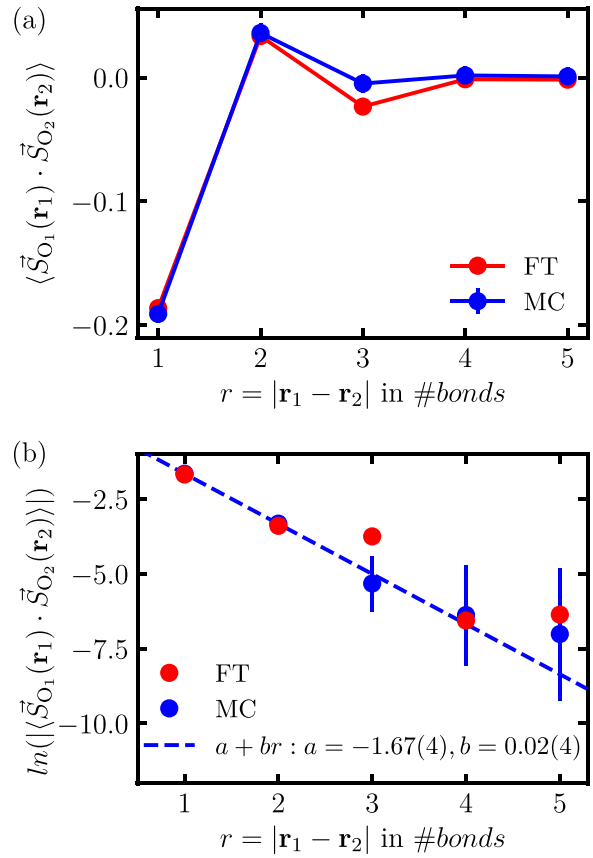

FIG. 4. Orphan spin correlations as a function of the number of bonds connecting two dilution clusters for systems containing $L^3 = 10^3$ (FT) and 12×4^3 (MC) spins at temperature $\beta = 1000$. (a) Orphan spin correlation function from FT and MC. (b) Logarithm of the absolute value of the orphan spin correlation function from MC and FT. The dashed blue line corresponds to the linear fit of the MC data. The close agreement between the data and fit indicates that the orphan spin correlations decay exponentially.

We confirm this estimate with MC simulations consisting of single-flip moves and the so-called short-loop moves described in Ref. [50]. Briefly, a short-loop move consists of randomly generating strings of spins of alternating signs along the lattice bonds. A loop is closed when an octahedron is revisited, while it is discarded if it encounters a defective octahedron in which the spins do not sum to zero. Flipping the spins belonging to an even loop length leaves all visited octahedra in a ground-state configuration. The shortest even loop, illustrated in Fig. 5(b), is formed by six spins. As shown in Fig. 5(a), the acceptance rate of single-flip moves drops to zero as the system reaches the ground state, while the acceptance rate for loop moves stabilizes at around 0.5, as only the loops with an even number of spins are accepted. To increase the acceptance rate of the loop moves, the algorithm

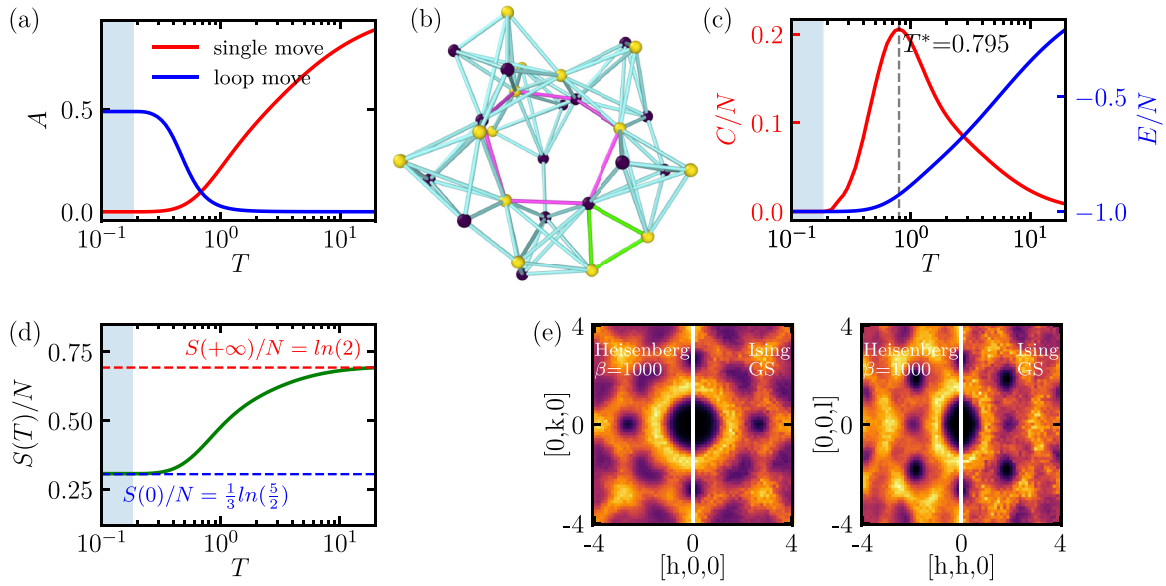

FIG. 5. (a) Acceptance rate A of single spin flips (red) and loop moves (blue) of the MC simulations for the Ising system as a function of temperature. The blue shaded area indicates the range of temperatures for which the acceptance rate of the single move vanishes. The acceptance rate for the loop moves also takes into account the probability of successfully forming such loops without visiting a defect octahedron. Since defect octahedra proliferate at high temperatures and loops cannot form, the acceptance rate for loop moves vanishes in that limit. (b) Exemplary ground-state configuration of the Ising model, where the yellow and black dots represent up and down spins, respectively. The bonds forming the shortest even length loop (six spins) are colored pink. The bonds forming the shortest loop (three spins) are colored green. Flipping all the spins belonging to an even loop generates a new ground-state configuration. (c) Specific heat and energy per spin as a function of temperature for the Ising model. (d) Entropy per site obtained by numerical integration of the specific heat from the MC simulations. The dashed blue line corresponds to the estimate of the entropy at zero temperature given by the Pauling counting argument. The dashed red line corresponds to the entropy at infinite temperature, obtained by counting all possible states. (e) Structure factor comparison between the Ising and Heisenberg models, obtained with MC simulations. The structure factor of the Heisenberg model is computed at the lowest simulated temperature, while that of the Ising model is computed in the ground-state manifold.

excludes the three-spin loop, which is also shown in Fig. 5(b). The specific heat in Fig. 5(c) features the characteristic bump of a disordered system connected to the high-temperature paramagnetic state. Figure 5(d) shows the entropy computed by numerically integrating the approximated thermodynamic relation

$$S(T) = S(+\infty) - \int_T^{+\infty} \frac{C(T')}{T'} dT'$$
$$\approx N \ln(2) - \int_T^{T_{\max}} \frac{C(T')}{T'} dT', \qquad (9)$$

where C is the specific heat obtained from the MC simulations. At low temperatures, the entropy agrees with the simple argument above. Furthermore, the static spin structure factor in Fig. 5(e) shows a pattern similar to that found for the Heisenberg case and the prediction from the SCGA calculation. We may thus conclude from this characterization that the Ising model does not order but possibly realizes a CSL state.

For a deeper theoretical understanding of the Ising case and, later, the quantum model, we may adopt an alternative perspective in which, instead of Ising spins on the trilline lattice, we identify the degrees of freedom as Ising variables at the midpoints of the bonds connecting the sites of the dual lattice, the trillium lattice. Thus, the system can be viewed as a dimer model on the trillium lattice where an up spin corresponds to a dimer placed on that bond while a down spin corresponds to no dimer. The ground-state condition of the trilline Ising model (corresponding to three spins up and three spins down in each octahedron) then translates into the condition of three dimers emanating from each trillium lattice site, the so-called triple dimer coverings. Crucially, the trillium lattice is *nonbipartite*. It was previously noted that dimer coverings on nonbipartite two-dimensional and 3D lattices can be distinguished by a $\mathbb{Z}_2$ winding parity [29,30,51]. The winding parity for 3D models like our trillium system can be explained in analogy to fluxes through a reference surface.

Let us consider a system with periodic boundaries along the x, y, and z directions. Furthermore, we choose a unit vector $\vec{e}_\mu$ ($\mu = x, y, z$) along one of these directions and a reference plane perpendicular to $\vec{e}_\mu$, which we denote Σ_μ and which extends over the full periodic system. We assume that the plane cuts N_μ dimers. Next, we consider a local move that keeps the system within the ground-state manifold. Such a move corresponds to switching the dimer occupation on a contractable loop of alternating occupation. If the loop does not pierce Σ_μ, the number of cut dimers N_μ remains unchained; otherwise, it will necessarily pierce the plane twice. The loop move may change the number of cut dimers N_μ, but the parity $N_\mu \pmod 2$ remains unchanged, establishing a $\mathbb{Z}_2$ topological index associated with the plane Σ_μ, or, more generally, associated with the direction $\vec{e}_\mu$. The argument is

analogous for the other two spatial directions, giving rise to $\mathbb{Z}_2$ flux sectors that establish a topological magnet. Thus, our Ising model corresponds to a $\mathbb{Z}_2$ CSL in three dimensions.

We may now upgrade our discussion to the quantum level by considering perturbations on top of the Ising ground states within degenerate perturbation theory. Such perturbations correspond to off-diagonal terms in the original S_i^z basis such as transverse fields $\Gamma \sum_i S_i^x$ and XY interaction terms $J_\perp \sum_{\langle i,j\rangle}(S_i^+ S_j^- + \text{H.c.})$, which flip spins and generically take the system out of the Ising ground-state manifold. Assuming $J \gg J_\perp, \Gamma$ such that defect octahedra have a large energy cost, the terms in the perturbation series are given by processes that lead the system from one ground state to the other. These processes, so-called loop resonances, correspond to the aforementioned flips of alternating spins on even length loops. At lowest order these are the six-site resonances illustrated in Fig. 5(b), and in the language of quantum dimer models we can write these perturbations as

$$H_{\text{QDM}} = \sum_{\hexagon} \Bigg\{ -t \left(\left| \quad \right\rangle \left\langle \quad \right| + \text{H.c.} \right) + v \left(\left| \quad \right\rangle \left\langle \quad \right| + \left| \quad \right\rangle \left\langle \quad \right| \right) \Bigg\}, \tag{10}$$

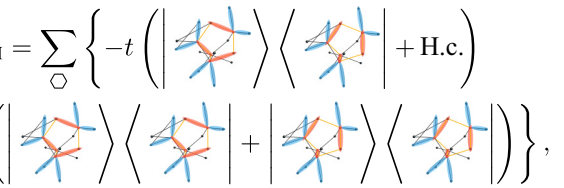

where we sum over all six-bond loops $\hexagon$ of the trillium lattice. Following Ref. [52], the resonance is of order $t \propto \Gamma^6/J^5$ or $-J_\perp^3/J^2$, where, for later arguments, we require a ferromagnetic $J_\perp < 0$. Furthermore, we have added a diagonal term with strength v [1,31,53,54] which counts the number of *flippable* loops in a given state. For negative $v \to -\infty$ this term generates a ground state with the maximal number of flippable loops, referred to as a columnar state. The opposite limit, $v \to \infty$, is characterized by no flippable loops and is generically called a staggered state. The phase diagram as a function of v/t is then generically divided into three regions. From a spin liquid perspective, the center region at $v/t \approx 1$ is the most interesting regime since it can give rise to emergent deconfined $U(1)$ or $\mathbb{Z}_2$ gauge theories [30].

Of particular importance is the RK point at $v = t$ [53], where we can rewrite the Hamiltonian as a sum of projectors:

$$H_{\text{RK}} = t \sum_{\hexagon} |\Phi_{\hexagon}\rangle \langle \Phi_{\hexagon}|, \quad |\Phi_{\hexagon}\rangle = \left| \quad \right\rangle - \left| \quad \right\rangle. \tag{11}$$

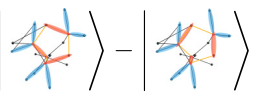

For positive t all eigenvalues are non-negative. Let us consider the classical Ising configurations, which, as described above, can be grouped into $\mathbb{Z}_2$ flux sectors. An application of the resonance term connects states only within each sector because the contractable loops are local moves. This allows us to define a state $|\Psi\rangle$ as an equal-weight superposition of all triple dimer coverings in the trillium lattice for each $\mathbb{Z}_2$ sector. Since $|\Psi\rangle$ is annihilated by each of the projectors $|\Phi_{\hexagon}\rangle \langle \Phi_{\hexagon}|$ in Eq. (11), the wave function $|\Psi\rangle$ is the exact and unique ground state in a given $\mathbb{Z}_2$ sector at the RK point. This argument assumes that all states in a $\mathbb{Z}_2$ sector are connected by resonance loops, which, however, is not always the case. For example, the dimer model on the triangular lattice contains staggered states disconnected from any other states [54]. In such cases only the connected states contribute to the equal-weight superposition in $|\Psi\rangle$, and different degenerate ground states in a $\mathbb{Z}_2$ sector exist. Since the minimal six-bond resonance loops of our trillium system are relatively short (of the same length as in pyrochlore spin ice), flippable loops are abundant, so that one can expect large connected sectors with spin liquid behavior.

Moreover, equal-time correlations are accessible at the RK point, which for an observable diagonal in the dimer basis can be calculated by an equal-weight summation over all triple dimer coverings, the same procedure as for the calculation of zero-temperature correlations in the pure Ising model. Thus, our zero-temperature MC results for the Ising model also hold for the quantum model at the RK point, and we can conclude that the latter system also has short-range and exponentially decaying correlations. Furthermore, physical configurations are distinguished by their $\mathbb{Z}_2$ winding parity characterizing the resulting state as a $\mathbb{Z}_2$ quantum spin liquid. The stability region of such a state is not clear from the above arguments, but following previous results for 3D dimer models in nonbipartite lattices a finite quantum spin liquid region in the phase diagram is possible [30].

To summarize, we have investigated the classical Ising model on the trilline lattice, derived from a fragile spin liquid model. We showed an absence of long-range correlations and the emergence of an extensively degenerate ground-state manifold characterized by a $\mathbb{Z}_2$ winding parity. Quantum mechanical perturbations on top of the ground state can be analyzed within the framework of quantum dimer models, for which we showed the emergence of a $\mathbb{Z}_2$ quantum spin liquid at the RK point.

VI. CONCLUSIONS

We constructed a classical Heisenberg model on the line graph of the trillium lattice, the trilline lattice, which has no order down to the lowest temperatures. We found exponentially decaying spin-spin correlations which manifest as a broad continuum in the spin structure factor. Moreover, we showed that such a state has a fractionalized magnetic response for a diluted system with nonmagnetic vacancies. Specifically, we found that the relevant vacancy clusters realize an effective $S/2$ free spin, characterizing the system as being distinctly different from a trivial paramagnet. Nevertheless, we confirmed with FT and MC calculations that such fractionalized charges are also short range correlated with a characteristic exponential decay. This is in contrast to the usual Coulomb spin liquids, which exhibit power-law correlations characteristic of the emergent gauge charges, for example, the monopoles of spin ice. Examining the Ising case, we again found an absence of ordering and an extensive ground-state degeneracy. Furthermore, by mapping the Ising model to triple dimer coverings on the trillium lattice we established the existence of $\mathbb{Z}_2$ flux sectors and found a $\mathbb{Z}_2$ quantum spin liquid state at the RK point of the system. We conclude from these results that our model realizes an instance of a fragile spin liquid in three dimensions.

Notably, the corner-sharing network of clusters in the trilline lattice, which gives rise to the fragile spin liquid, is realized on the distorted windmill lattice when the Heisenberg interactions between the first and fourth neighbors are all equal and antiferromagnetic, as explained in Appendix B. This suggests that materials with interactions close to this fine-tuned point may, indeed, exist. Promising candidates can be found in the compound family $A\mathrm{CuTe_2O_6}$ ($A = \mathrm{Sr}^{2+}, \mathrm{Pb}^{2+}, \mathrm{Ba}^{2+}$), which realizes a distorted windmill lattice with antiferromagnetic and isotropic couplings [27,55,56]. In principle, however, the phenomena discussed in this work require all couplings within the corner-sharing octahedra to be identical. A finite difference $\Delta J \neq 0$ between the strengths of these octahedron couplings leads to a finite bandwidth $\sim\Delta J$ for the formerly flat bands. In the generic case, ΔJ selects specific states from the extensive ground-state manifold, so the system develops magnetic long-range order at a critical temperature $T_c \sim \Delta J$. However, for sufficiently small ΔJ one expects effective fragile spin liquid behavior to survive in the temperature regime $\Delta J < T < J$, where the first inequality ensures that thermal fluctuations wipe out any effect of the perturbation ΔJ, while the second inequality guarantees zero spin sums in the octahedra (note that here J refers to the *average* of the octahedron couplings). Beyond the purely classical spin model discussed here, quantum fluctuation could further help to stabilize spin liquid phases, possibly down to $T = 0$ even at finite ΔJ. This is particularly relevant for the aforementioned family of compounds, in which quantum fluctuations are expected to play a significant role, as they feature spin $S = 1/2$. Finally, while the fragile spin liquid is a concept defined for classical spins, the full quantum Heisenberg version of this model remains unexplored and thus presents an interesting direction for future research.

ACKNOWLEDGMENTS

We are grateful to B. Doucot for fruitful discussions. This work was in part supported by the Deutsche Forschungsgemeinschaft under Grant No. SFB 1143 (Project No. 247310070) and the Cluster of Excellence ct.qmat (EXC 2147, Project No. 390858490). J.R. acknowledges support from the Deutsche Forschungsgemeinschaft within Project ID No. 277101999 CRC 183 (Project No. A04). The work of J. R. was performed, in part, at the Aspen Center for Physics, which is supported by National Science Foundation Grant No. PHY-2210452. The MC simulations were performed on the Sheldon cluster at the Physics Department of Freie Universität Berlin.

APPENDIX A: DETAILS ON THE MONTE CARLO SIMULATIONS

We simulate a system of $N = 12 \times L \times L \times L$ spins with periodic boundary conditions. The spins are initialized in a random configuration and gradually cooled down. For the MC simulations of the Heisenberg model, the initial temperature is set to $T = 10$, as in the main text T is expressed in units of J with $J = 1$. A single MC move consists of N heat bath moves [57], each followed by 10 over-relaxation moves [58]. The results in Figs. 2(c), 2(d) and 3 were obtained by simulating a linear size $L = 8$ and averaging over 100 independent runs. The results in Fig. 4 were obtained by simulating a linear size $L = 4$ and averaging over 500 independent runs. The error bars correspond to the standard deviation across the runs.

For the MC simulations of the Ising model, the initial temperature is set to $T = 20$, and a single MC move consists of N single spin flip moves and N loop moves, as described in Sec. V. Both types of moves are accepted or rejected according to the Metropolis scheme. When the temperature at which single flip moves are always rejected is reached, only loop moves are applied. The results in Fig. 5 were obtained by simulating a linear size $L = 8$ and averaging over 100 independent runs.

APPENDIX B: CONSTRUCTION OF THE TRILLINE LATTICE

The trilline lattice is constructed by first identifying all the nearest-neighbor bonds in the original trillium lattice. The trillium lattice is a simple cubic lattice with four sites in the unit cell, whose positions depend on a real parameter u [37]. The midpoints of these bonds correspond to the sites of the trilline lattice. Equal Heisenberg interactions are assigned to all pairs of trilline sites, corresponding to the midpoints of the bonds originating from the same trillium lattice point. Alternatively, a specific realization of the trilline lattice can be constructed starting from a distorted version of the hyperkagome lattice, known as the distorted windmill lattice. The distorted windmill lattice is based on a simple cubic lattice with 12 sites in the unit cell, whose positions depend on a real parameter y [59]. To construct the trilline lattice, we fix the value of y equal to that of $\mathrm{PbCuTe_2O_6}$ and consider an antiferromagnetic Heisenberg model with equal-strength interactions extending up to the fourth nearest neighbor $J_1 = J_2 = J_3 = J_4$ [28]. These interactions form a network of distorted octahedra, whose centers form a trillium with lattice parameter $u = 7/8$. This construction can be generalized to other values of y, provided that the network formed by the couplings remains unchanged. In this work, we adopt the latter construction.

APPENDIX C: DETAILS OF THE ANALYTICAL CALCULATIONS

The calculations for the Heisenberg model in Eq. (1) were carried out within the framework of the self-consistent Gaussian approximation and vacancy FT. For this, we followed Refs. [20,34,35,38–40]. In particular, the calculations for the orphan spin magnetic moment and the spatial correlations are concisely shown in the Supplemental Material of Ref. [20]. Although the analysis proceeds directly, we present here the form of $J_{ab}(\mathbf{q})$ in the unit cell basis for reproducibility:

$$\begin{pmatrix}
2 & 1+e^{-iq_x} & 1 & 1 & 1 & e^{i(q_y-q_z)} & e^{-iq_z} & 0 & e^{-iq_z} & e^{i(-q_x+q_y)} & e^{i(-q_x+q_y-q_z)} & 0 \\
1+e^{iq_x} & 2 & 1 & 1 & 1 & e^{i(q_x+q_y-q_z)} & e^{i(q_x-q_z)} & 0 & e^{-iq_z} & e^{iq_y} & e^{i(q_y-q_z)} & 0 \\
1 & 1 & 2 & 1 & 1 & 1 & 1 & 1 & 1+e^{-iq_z} & 0 & 0 & e^{-iq_x} \\
1 & 1 & 1 & 2 & 1+e^{-iq_y} & 0 & 0 & 1 & e^{-iq_z} & 1 & 1 & 1 \\
1 & 1 & 1 & 1+e^{iq_y} & 2 & 0 & 0 & e^{iq_y} & e^{-iq_z} & e^{iq_y} & e^{iq_y} & e^{iq_y} \\
e^{i(q_z-q_y)} & e^{i(-q_x-q_y+q_z)} & 1 & 0 & 0 & 2 & 1+e^{-iq_y} & 1 & 1 & e^{i(-q_x+q_z)} & e^{-iq_x} & e^{-iq_x} \\
e^{iq_z} & e^{i(-q_x+q_z)} & 1 & 0 & 0 & 1+e^{iq_y} & 2 & 1 & 1 & e^{i(-q_x+q_y+q_z)} & e^{i(-q_x+q_y)} & e^{-iq_x} \\
0 & 0 & 1 & 1 & e^{-iq_y} & 1 & 1 & 2 & 1 & 1 & 1 & 1+e^{-iq_x} \\
e^{iq_z} & e^{iq_z} & 1+e^{iq_z} & e^{iq_z} & e^{iq_z} & 1 & 1 & 1 & 2 & 0 & 0 & e^{-iq_x} \\
e^{i(q_x-q_y)} & e^{-iq_y} & 0 & 1 & e^{-iq_y} & e^{i(q_x-q_z)} & e^{i(q_x-q_y-q_z)} & 1 & 0 & 2 & 1+e^{-iq_z} & 1 \\
e^{i(q_x-q_y+q_z)} & e^{i(-q_y+q_z)} & 0 & 1 & e^{-iq_y} & e^{iq_x} & e^{i(q_x-q_y)} & 1 & 0 & 1+e^{iq_z} & 2 & 1 \\
0 & 0 & e^{iq_x} & 1 & e^{-iq_y} & e^{iq_x} & e^{iq_x} & 1+e^{iq_x} & e^{iq_x} & 1 & 1 & 2
\end{pmatrix}. \quad \text{(C1)}$$

[1] P. W. Anderson, Resonating valence bonds: A new kind of insulator? Mater. Res. Bull. **8**, 153 (1973).

[2] L. Balents, Spin liquids in frustrated magnets, Nature (London) **464**, 199 (2010).

[3] Y. Zhou, K. Kanoda, and T.-K. Ng, Quantum spin liquid states, Rev. Mod. Phys. **89**, 025003 (2017).

[4] X.-G. Wen, Quantum orders and symmetric spin liquids, Phys. Rev. B **65**, 165113 (2002).

[5] C. Castelnovo, R. Moessner, and S. Sondhi, Spin ice, fractionalization, and topological order, Annu. Rev. Condens. Matter Phys. **3**, 35 (2012).

[6] J. Knolle and R. Moessner, A field guide to spin liquids, Annu. Rev. Condens. Matter Phys. **10**, 451 (2019).

[7] C. Xu, Gapless bosonic excitation without symmetry breaking: An algebraic spin liquid with soft gravitons, Phys. Rev. B **74**, 224433 (2006).

[8] C. Chamon, Quantum glassiness in strongly correlated clean systems: An example of topological overprotection, Phys. Rev. Lett. **94**, 040402 (2005).

[9] J. Haah, Local stabilizer codes in three dimensions without string logical operators, Phys. Rev. A **83**, 042330 (2011).

[10] S. Vijay, J. Haah, and L. Fu, Fracton topological order, generalized lattice gauge theory, and duality, Phys. Rev. B **94**, 235157 (2016).

[11] S. Vijay, J. Haah, and L. Fu, A new kind of topological quantum order: A dimensional hierarchy of quasiparticles built from stationary excitations, Phys. Rev. B **92**, 235136 (2015).

[12] G. B. Halász, T. H. Hsieh, and L. Balents, Fracton topological phases from strongly coupled spin chains, Phys. Rev. Lett. **119**, 257202 (2017).

[13] Y. You and F. von Oppen, Building fracton phases by Majorana manipulation, Phys. Rev. Res. **1**, 013011 (2019).

[14] C. Xu and M. P. A. Fisher, Bond algebraic liquid phase in strongly correlated multiflavor cold atom systems, Phys. Rev. B **75**, 104428 (2007).

[15] C. Xu and P. Hořava, Emergent gravity at a Lifshitz point from a Bose liquid on the lattice, Phys. Rev. D **81**, 104033 (2010).

[16] O. Benton, L. D. C. Jaubert, H. Yan, and N. Shannon, A spin-liquid with pinch-line singularities on the pyrochlore lattice, Nat. Commun. **7**, 11572 (2016).

[17] O. Benton and R. Moessner, Topological route to new and unusual Coulomb spin liquids, Phys. Rev. Lett. **127**, 107202 (2021).

[18] M. Pretko, Generalized electromagnetism of subdimensional particles: A spin liquid story, Phys. Rev. B **96**, 035119 (2017).

[19] H. Yan, O. Benton, L. D. C. Jaubert, and N. Shannon, Rank–2 $U(1)$ spin liquid on the breathing pyrochlore lattice, Phys. Rev. Lett. **124**, 127203 (2020).

[20] R. Flores-Calderón, O. Benton, and R. Moessner, Irrational moments and signatures of higher-rank gauge theories in diluted classical spin liquids, Phys. Rev. Lett. **133**, 106501 (2024).

[21] H. Yan, O. Benton, A. H. Nevidomskyy, and R. Moessner, Classification of classical spin liquids: Detailed formalism and suite of examples, Phys. Rev. B **109**, 174421 (2024).

[22] H. Yan, O. Benton, R. Moessner, and A. H. Nevidomskyy, Classification of classical spin liquids: Typology and resulting landscape, Phys. Rev. B **110**, L020402 (2024).

[23] A. Kitaev, Anyons in an exactly solved model and beyond, Ann. Phys. (NY) **321**, 2 (2006).

[24] E. Dennis, A. Kitaev, A. Landahl, and J. Preskill, Topological quantum memory, J. Math. Phys. **43**, 4452 (2002).

[25] X. G. Wen, Mean-field theory of spin-liquid states with finite energy gap and topological orders, Phys. Rev. B **44**, 2664 (1991).

[26] M. A. Levin and X.-G. Wen, String-net condensation: A physical mechanism for topological phases, Phys. Rev. B **71**, 045110 (2005).

[27] S. Chillal, Y. Iqbal, H. O. Jeschke, J. A. Rodriguez-Rivera, R. Bewley, P. Manuel, D. Khalyavin, P. Steffens, R. Thomale, A. Islam *et al.*, Evidence for a three-dimensional quantum spin liquid in $PbCuTe_2O_6$, Nat. Commun. **11**, 2348 (2020).

[28] A. Fancelli, J. Reuther, and B. Lake, Classical spin models of the windmill lattice and their relevance for $PbCuTe_2O_6$, Phys. Rev. B **108**, 184415 (2023).

[29] J. Rehn, A. Sen, and R. Moessner, Fractionalized $\mathbb{Z}_2$ classical Heisenberg spin liquids, Phys. Rev. Lett. **118**, 047201 (2017).

[30] D. A. Huse, W. Krauth, R. Moessner, and S. L. Sondhi, Coulomb and liquid dimer models in three dimensions, Phys. Rev. Lett. **91**, 167004 (2003).

[31] P. Fendley, R. Moessner, and S. L. Sondhi, Classical dimers on the triangular lattice, Phys. Rev. B **66**, 214513 (2002).

[32] G. Misguich, D. Serban, and V. Pasquier, Quantum dimer model on the kagome lattice: Solvable dimer-liquid and Ising gauge theory, Phys. Rev. Lett. **89**, 137202 (2002).

[33] A. Sen, K. Damle, and R. Moessner, Fractional spin textures in the frustrated magnet $SrCr_{9p}Ga_{12-9p}O_{19}$, Phys. Rev. Lett. **106**, 127203 (2011).

[34] J. Rehn, A. Sen, K. Damle, and R. Moessner, Classical spin liquid on the maximally frustrated honeycomb lattice, Phys. Rev. Lett. **117**, 167201 (2016).

[35] A. Sen, K. Damle, and R. Moessner, Vacancy-induced spin textures and their interactions in a classical spin liquid, Phys. Rev. B **86**, 205134 (2012).

[36] P. Patil, F. Alet, S. Capponi, and K. Damle, Quantum half-orphans in kagome antiferromagnets, Phys. Rev. Res. **2**, 043425 (2020).

[37] J. M. Hopkinson and H.-Y. Kee, Geometric frustration inherent to the trillium lattice, a sublattice of the B20 structure, Phys. Rev. B **74**, 224441 (2006).

[38] D. A. Garanin and B. Canals, Classical spin liquid: Exact solution for the infinite-component antiferromagnetic model on the kagomé lattice, Phys. Rev. B **59**, 443 (1999).

[39] S. V. Isakov, R. Moessner, and S. L. Sondhi, Why spin ice obeys the ice rules, Phys. Rev. Lett. **95**, 217201 (2005).

[40] S. V. Isakov, K. Gregor, R. Moessner, and S. L. Sondhi, Dipolar spin correlations in classical pyrochlore magnets, Phys. Rev. Lett. **93**, 167204 (2004).

[41] F.-Y. Li, Y.-D. Li, Y. B. Kim, L. Balents, Y. Yu, and G. Chen, Weyl magnons in breathing pyrochlore antiferromagnets, Nat. Commun. **7**, 12691 (2016).

[42] R. Moessner and J. T. Chalker, Properties of a classical spin liquid: The Heisenberg pyrochlore antiferromagnet, Phys. Rev. Lett. **80**, 2929 (1998).

[43] R. Moessner and J. T. Chalker, Low-temperature properties of classical geometrically frustrated antiferromagnets, Phys. Rev. B **58**, 12049 (1998).

[44] R. Moessner and A. J. Berlinsky, Magnetic susceptibility of diluted pyrochlore and $SrCr_{9-9x}Ga_{3+9x}O_{19}$ antiferromagnets, Phys. Rev. Lett. **83**, 3293 (1999).

[45] G. André, R. Bidaux, J.-P. Carton, R. Conte, and L. de Seze, Frustration in periodic systems: Exact results for some 2D Ising models, J. Phys. (Paris) **40**, 479 (1979).

[46] D. A. Garanin, Self-consistent Gaussian approximation for classical spin systems: Thermodynamics, Phys. Rev. B **53**, 11593 (1996).

[47] For simplicity we omit the vector notation for the $\mathcal{N}$-component spins in this section. Within this constraint formalism the different spin components can be viewed as independent degrees of freedom such that a distinction between different components is not necessary.

[48] J. Rehn, A. Sen, A. Andreanov, K. Damle, R. Moessner, and A. Scardicchio, Random Coulomb antiferromagnets: From diluted spin liquids to Euclidean random matrices, Phys. Rev. B **92**, 085144 (2015).

[49] A. Sen and R. Moessner, Topological spin glass in diluted spin ice, Phys. Rev. Lett. **114**, 247207 (2015).

[50] R. G. Melko and M. J. P. Gingras, Monte Carlo studies of the dipolar spin ice model, J. Phys.: Condens. Matter **16**, R1277 (2004).

[51] R. Moessner and S. L. Sondhi, Three-dimensional resonating-valence-bond liquids and their excitations, Phys. Rev. B **68**, 184512 (2003).

[52] M. Hermele, M. P. A. Fisher, and L. Balents, Pyrochlore photons: The $U(1)$ spin liquid in a $s = 1/2$ three-dimensional frustrated magnet, Phys. Rev. B **69**, 064404 (2004).

[53] D. S. Rokhsar and S. A. Kivelson, Superconductivity and the quantum hard-core dimer gas, Phys. Rev. Lett. **61**, 2376 (1988).

[54] R. Moessner and S. L. Sondhi, Resonating valence bond phase in the triangular lattice quantum dimer model, Phys. Rev. Lett. **86**, 1881 (2001).

[55] S. Chillal, A. T. M. N. Islam, H. Luetkens, E. Canévet, Y. Skourski, D. Khalyavin, and B. Lake, Magnetic structure of the quantum magnet $SrCuTe_2O_6$, Phys. Rev. B **102**, 224424 (2020).

[56] A. Samartzis, S. Chillal, H. O. Jeschke, D. J. Voneshen, Z. Lu, A. T. M. N. Islam, and B. Lake, Magnetic excitation spectrum and Hamiltonian of the quantum spin chain compound $BaCuTe_2O_6$, Phys. Rev. B **107**, 184435 (2023).

[57] Y. Miyatake, M. Yamamoto, J. J. Kim, M. Toyonaga, and O. Nagai, On the implementation of the 'heat bath' algorithms for Monte Carlo simulations of classical Heisenberg spin systems, J. Phys. C **19**, 2539 (1986).

[58] M. Creutz, Overrelaxation and Monte Carlo simulation, Phys. Rev. D **36**, 515 (1987).

[59] S. V. Isakov, J. M. Hopkinson, and H.-Y. Kee, Fate of partial order on trillium and distorted windmill lattices, Phys. Rev. B **78**, 014404 (2008).